On equations of state in a lattice Boltzmann method☆

A.L. Kupershtokh *, D.A. Medvedev, D.I. Karpov

Lavrentyev Institute of Hydrodynamics of Siberian Branch of Russian Academy of Sciences, Lavrentyev prosp. 15, Novosibirsk, 630090, Russia

ARTICLE INFO

ABSTRACT

We investigate the use of various equations of state (EOS) in the single-component multiphase lattice Boltzmann model. Several EOS are explored: van der Waals, Carnahan–Starling and Kaplun–Meshalkin EOS [A.B. Kaplun, A.B. Meshalkin, Thermodynamic validation of the form of unified equation of state for liquid and gas, High Temperature 41 (3) (2003) 319–326]. The last one was modified in order to obtain the correct critical point. The Carnahan–Starling and modified Kaplun–Meshalkin EOS are in better agreement with the experimental data on coexistence curves than the van der Waals EOS.

It is shown that the approximation of the gradient of special potential is crucial to obtain the correct coexistence curve, especially its low-density part. The correct method of incorporating the body forces into the lattice Boltzmann model is also very important. We propose a new scheme which allows us to obtain large density ratio (up to 10^9 in the stationary case) and to reproduce the coexistence curve with high accuracy. The spurious currents at vapor–liquid interface are also greatly reduced.

1. Introduction

Simulation of multiphase flows (flows with possible phase transitions between liquid and gas phases) is a frequent problem in scientific and industrial applications. Mesoscopic methods such as lattice Boltzmann equation (LBE) method are especially useful for such problems because they do not require tracking the interfaces that can appear, disappear and undergo topological changes. To simulate such flows, one needs an equation of state accurately describing both liquid and gas phases, and their coexistence curve. The numeric implementation of the selected equation of state should lead to stable solutions over a broad range of temperature and should be sufficiently simple.

There are three commonly used approaches to simulation of phase transitions by an LBE method. The first approach introduced in [1] uses explicit interparticle interactions. The second one is based on the free energy [2]. This approach ensures the constant interface thickness. However, in this case, the temperature dependence of the surface tension is incorrect. In the third approach [3], the total force acting on the fluid at a node is expressed as a gradient of special potential. In some special cases, the third approach coincides with the first one. In the present work, we employed the third approach because it allows one to incorporate easily an arbitrary form of EOS.

There are several known problems with use of different EOS in the LBE method. First, the coexistence curve obtained in simulations differs from the theoretical one, the difference increases when we go farther from the critical temperature. Second, large spurious currents are produced at vapor–liquid interface in simulations. Because of both these effects, the simulations are stable in a narrow range of temperature only, and ratios of the liquid density to the vapor density are not very high. The density ratio of 10^3 can be obtained using an additional order parameter with its own evolution equation [4,
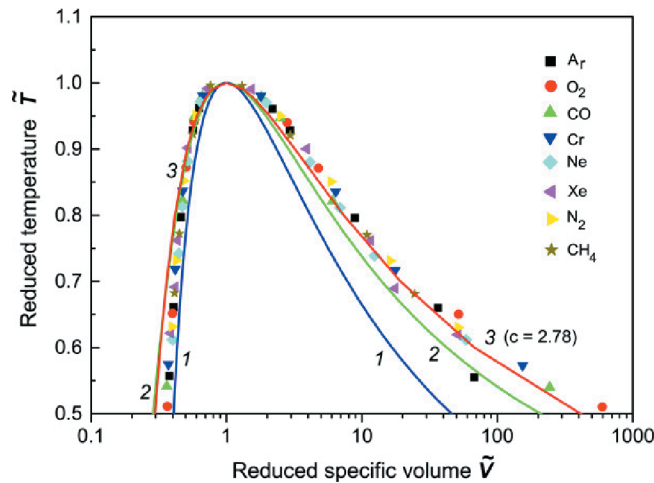
Fig. 1. Coexistence curves. Curve *1*—vdW EOS, curve *2*—C–S EOS, curve *3*—mKM EOS for $c = 2.78$, symbols—experimental data [18].

5] or a special form of the free energy approximation [6]. However, in all these works, no well-defined EOS (such as vdW) was recovered. Also, the coexistence curve was very far from the one of real fluids. Spurious currents can be reduced to a certain extent by use of higher-order approximation of the gradient term [7,8]. This requires some additional computations and leads to more complicated boundary conditions. These problems are well illustrated in the papers [7,9,10]. Authors of the last paper even stated that the van der Waals equation is not suitable for a liquid–vapor system with temperatures much lower than the critical one. It was shown in works [11,12] that the exact difference method [11,13,14] should be used to incorporate the body force term into LBE at simulations of phase transitions. In the present paper, we show that rather low maximum ratio of liquid and vapor densities, deviations of the coexistence curves from theoretical ones and large spurious velocities obtained in the work of Yuan and Schaefer [10] are caused not by the peculiarities of the EOS itself but by inaccuracy of methods usually involved in the modeling of phase transitions by LBE.

The paper is organized as follows. In Section 2, we review the equations of state used and compare their properties with the properties of real substances. In Section 3, the exact difference method to include body force into an LBE, and the new numerical approximation of the potential gradient are described. In Section 4, we compare the results provided with different methods and show that our method has the best performance. Application of the method to several different problems is also presented. Some concluding remarks are given in Section 5.

2. Equations of state

Many equations of state are available which describe both the liquid and gaseous phases of a fluid. Historically, one of the first EOS was proposed by van der Waals. It has the form:

$$P = \frac{RT}{V - B} - \frac{A}{V^2},\qquad(1)$$

where P is the pressure, V is the specific volume, and T is the temperature. Instead of V, one can use the density $\rho = 1/V$. Coefficients A and B should be fitted for every fluid from the experiments. This equation of state is popular because of its clear physical interpretation and simple cubic density dependence of the pressure.

To make the EOS more general, it is useful to apply non-dimensional (reduced) variables $\tilde{P} = P/P_c$, $\tilde{\rho} = \rho/\rho_c$, $\tilde{T} = T/T_c$ where P_c, ρ_c, and T_c are the values of pressure, density and temperature in the critical point. Using the reduced variables, the van der Waals (vdW) EOS can be written in the form:

$$\tilde{P} = \frac{8\tilde{\rho}\tilde{T}}{3 - \tilde{\rho}} - 3\tilde{\rho}^2.\qquad(2)$$

This equation has no free parameters, hence, it can describe properties of real fluids only qualitatively (Fig. 1). On the other hand, this EOS is very simple.

There are several generalizations of the vdW EOS. One of them is the Carnahan–Starling (C–S) EOS, which can be written in reduced variables as

$$\tilde{P} = c\tilde{\rho}\tilde{T}\frac{1 + b\tilde{\rho} + (b\tilde{\rho})^2 - (b\tilde{\rho})^3}{(1 - b\tilde{\rho})^3} - a\tilde{\rho}^2.\qquad(3)$$

Three conditions in the critical point (at $\tilde{\rho} = 1$ and $\tilde{T} = 1$) should be satisfied

$$\tilde{P} = 1, \qquad \left(\frac{\partial\tilde{P}}{\partial\tilde{\rho}}\right)_{\tilde{T}} = 0, \qquad \left(\frac{\partial^2\tilde{P}}{\partial\tilde{\rho}^2}\right)_{\tilde{T}} = 0.\qquad(4)$$

From these equations, values of a, b and c can be calculated

$$a = 3.852462257, \qquad b = 0.1304438842, \qquad c = 2.785855166.$$

There are no free parameters in the C–S EOS. The C–S EOS is in better agreement with experimental data on coexistence curves than the vdW EOS, but the discrepancies at the vapor branch are relatively large (Fig. 1). Nevertheless, it is one of the best analytical EOS describing most accurately the behavior of the rigid-spheres model [15].

The last EOS we considered is the EOS derived recently by Kaplun and Meshalkin [16,17]:

$$P = \frac{RT}{V} \left(1 + \frac{C}{V - B} \right) - \frac{A}{V^2}. \tag{5}$$

For $C = B$, this equation coincides with the vdW EOS (1). Constants A, B, C were obtained in [16,17] by fitting the experimental data in a wide range of parameters. Unfortunately, for parameters given in [16], the critical point does not coincide with the real one. Using the reduced variables, this equation can be written as

$$\tilde{P} = c\tilde{\rho}\tilde{T} \left(1 + \frac{d}{1/\tilde{\rho} - b} \right) - a\tilde{\rho}^2. \tag{6}$$

To calculate the values of parameters that ensure the unities of reduced variables in the critical point we used three conditions (4). Hence, we obtain relations between parameters a, b, c, d

$$a = \frac{1}{3 - c}, \qquad b = 3 - c, \qquad d = \frac{12c - 6c^2 + c^3 - 8}{c(3 - c)}.$$

The EOS (6) with these relations between parameters could be named the modified Kaplun–Meshalkin EOS (mKM EOS). One of these four parameters is free. We choose c to be this one. If we set $c = 8/3$, we obtain the vdW EOS. For the best agreement with experimental data on the coexistence curve, the value $c = 2.78$ should be chosen (see Fig. 1).

Fig. 1 shows the coexistence curves for the vdW, mKM and C–S EOS along with the experimental data on several fluids [18]. The liquid branch of the coexistence curve is reproduced equally well with all three EOS. For the vapor branch, the mKM EOS has the best agreement with the experiment, and the vdW EOS has the worst one. Thus, we consider the modified KM EOS to be very convenient for the modeling of two-phase flows because it has simple analytical form and approximates quite well the experimental data on a large set of fluids in a wide range of parameters of state.

3. Numerical method

3.1. Lattice Boltzmann equation method

In the lattice Boltzmann equation method, the fluid is represented by a collection of pseudoparticles that move on a regular spatial lattice and undergo collisions at its nodes. The discrete set of velocity vectors $\mathbf{c}_k$, $k = 0, \ldots, N$ is possible. One-particle distribution functions f_k are used as main variables. Lattice vectors $\mathbf{e}_k$ are equal to $\mathbf{e}_k = \mathbf{c}_k \Delta t$, where Δt is the time step. The evolution equation is written as

$$f_k(\mathbf{x} + \mathbf{e}_k, t + \Delta t) = f_k(\mathbf{x}, t) + \Omega_k + \Delta f_k. \tag{7}$$

Here, Δf_k is the body force term. We used the BGK-form of collision operator [19] $\Omega_k = \left(f_k^{eq} - f_k \right) / \tau$, but other forms are also possible.

The fluid density ρ and the velocity $\mathbf{u}$ at a node (in the absence of body force term) can be calculated as

$$\rho = \sum_{k=0}^{N} f_k, \qquad \rho\mathbf{u} = \sum_{k=0}^{N} \mathbf{c}_k f_k. \tag{8}$$

If special body forces acting on a fluid (see Section 3.3) are absent in (7), the equation of state for this model has the form like that for an ideal gas

$$P = \rho\theta. \tag{9}$$

The "kinetic temperature" θ of LBE pseudoparticles depends on the specific LB model used. For usual models D1Q3, D2Q9 and D3Q19, $\theta = (h/\Delta t)^2/3$, where h is the lattice spacing. Often, lattice spacing and time step are taken as unities in LBE simulations.

3.2. Body forces in LBE: Exact difference method

Flows with body forces acting on a fluid are ubiquitous. These forces can be gravity (in thermal convection), electric forces (electrohydrodynamic flows) and so on. In all cases, the correct incorporation of the action of forces into an LBE method is necessary. There are many methods to include forces in LBE simulations [1,20–24]. While all these methods satisfy the conservation laws of mass and momentum, they are correct only in the first order on $\Delta\mathbf{u} = \mathbf{F}\Delta t/\rho$ as was shown in [11, 13,14]. Here, $\Delta\mathbf{u}$ is the change of the mass velocity at a node during time step Δt. The discrepancies in the higher-order
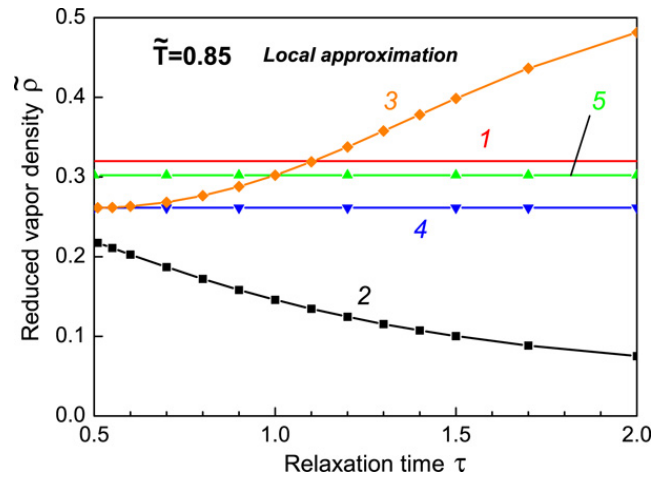
Fig. 2. Vapor density at coexistence curve for the vdW EOS vs. relaxation time. Curve *1*—theory (Maxwell rule), curve *2*—method of explicit derivative [20–23], curve *3*—method of modification of collision operator [1], curve *4*—combined method [24], curve *5*—our method of exact difference.

terms lead to incorrect values of distribution functions, and the internal energy does not correspond to the temperature, which should be equal to $\theta = (h/\Delta t)^2/3$ in isothermal LBE models. Error in the internal energy results in incorrect values of the density and the pressure in the areas where the force acted producing several unphysical effects such as oscillations in time [14].

Correct implementation of the body force term is especially necessary in the multiphase simulations because forces (and velocity changes) inside the liquid–vapor transition layer are not small. A new method to take into account body forces was proposed in [11,13,14], the exact difference method (EDM). This method was derived directly from the Boltzmann equation. At small Knudsen number, the body force term in Boltzmann equation can be rewritten (in the same order of approximation as in other methods) as a full derivative of the equilibrium distribution function along the Lagrange coordinate $\mathrm{d}f^{eq}(\rho, \mathbf{u})/\mathrm{d}t$ at constant density ρ. After discretization of the Boltzmann equation in the velocity space we derived EDM for LBE in the form

$$\Delta f_k = f_k^{eq}(\rho, \mathbf{u} + \Delta\mathbf{u}) - f_k^{eq}(\rho, \mathbf{u}), \tag{10}$$

where $\Delta\mathbf{u} = \mathbf{F}\Delta t/\rho$. The body force term Δf_k is simply equal to a difference of equilibrium distribution functions corresponding to the mass velocity after and before the action of a force during time step at constant density ρ. In this case, instead of (8), the real fluid velocity should be taken at half time step [25]

$$\rho\mathbf{u} = \sum_{k=0}^{N} \mathbf{c}_k f_k + \mathbf{F}\Delta t/2.$$

Since the method of exact difference was derived in [11,13,14] directly from the Boltzmann equation, the EDM can be used not only for the BGK collision operator but for arbitrary form of collision term (particularly, for the multiple-relaxation-time collision operator).

In order to demonstrate the importance of the correct implementation of the body force term, we simulated the coexistence of liquid and vapor for a fluid with the vdW EOS. The vapor density obtained in simulation at $\tilde{T} = 0.85$ for different relaxation time τ is plotted in Fig. 2 along with the theoretical value obtained from the Maxwell rule. All LBE calculations were performed using local approximation (19). For the methods of explicit derivative [20–23] and the method of modification of the collision operator [1], the vapor density changes with the change of τ that is unphysical. The combined method of Guo et al. [24] gives results independent on τ but rather different from theoretical values. Only the results obtained using the EDM agree well with the theory and do not depend on relaxation time.

3.3. Special forces for simulating the vapor–liquid phase transition

In LBE methods, different phases are simulated uniformly. Hence, there is no need in an explicit interface tracking. Boundaries between liquid and gas are represented as thin transition layers of finite width (several lattice nodes) where density changes smoothly from one bulk value to another. In the works [1,26], the special mesoscopic forces acting between every pair of neighbor nodes were introduced to simulate these transition layers. The total force acting on a fluid at a node is equal to

$$\mathbf{F}(\mathbf{x}) = \psi(\rho(\mathbf{x})) \sum_{k=1}^{N} G_k \psi(\rho(\mathbf{x} + \mathbf{e}_k))\mathbf{e}_k. \tag{11}$$

Here, G_k are the coefficients for basic and diagonal directions, "effective mass" $\psi(\rho)$ is an increasing function of density. All coefficients G_k corresponding to basic directions are equal to $G_k = G_1$. The forces in Eq. (11) are attractive for $G_1 > 0$. The

equation of state for this model has the form

$$P = \rho\theta - \alpha G_1 \psi^2. \tag{12}$$

Coefficients G_k for diagonal directions and numerical coefficient α depend on the model used. The coefficient α is equal to $\alpha = 1$ in the model D1Q3, $\alpha = 3/2$ in the model D2Q9, and $\alpha = 3$ in the model D3Q19. The coefficients G_k for diagonal directions are equal to $G_k = G_1/4$ in the model D2Q9, and $G_k = G_1/2$ in the model D3Q19. For certain forms of the function $\psi(\rho)$, the equation of state (12) allows a phase transition in this isothermal model. Particularly, the phase transition is possible for the function proposed in [1,26]

$$\psi(\rho) = \rho_0(1 - \exp(-\rho/\rho_0)),$$

if the value of G_1 is greater than the critical value $G_{1*} = 2\theta/(\alpha\rho_0)$.

In the work [3], Zhang and Chen proposed another method to include arbitrary EOS in an LBE method. In this method, the total force acting on the fluid at a node is expressed as a gradient of special potential which can be written using the EOS

$$\mathbf{F} = -\nabla U, \quad U = P(\rho, T) - \rho\theta. \tag{13}$$

Since we use the reduced variables in simulations, we need to match physical units and lattice units. Hence, the potential U should be also written in reduced variables $\tilde{U} = U\Delta t^2/(\rho_c h^2)$. In this case, it is expressed as

$$\tilde{U} = k\tilde{P}(\tilde{\rho}, \tilde{T}) - \tilde{\rho}\tilde{\theta}, \tag{14}$$

where $\tilde{\theta} = \theta(\Delta t/h)^2 = 1/3$. The coefficient k is equal to

$$k = \frac{P_c}{\rho_c}\frac{\Delta t^2}{h^2}.$$

If we take $h/\Delta t = 10^3$ m/s, then this coefficient is equal to $k = 0.00915$ for argon. For other inert gases, it is also of the order of 0.01. These values were used in the rest of the paper.

In the framework of isothermal LBE models [1,26], the following formula for the function $\psi(\rho)$ was obtained in [27,28]

$$\psi(\rho) = \sqrt{\frac{-(P(\rho) - \rho\theta)}{\alpha G_1}}$$

for equations of state in the form $P = P(\rho)$. We proposed in [12,29,30] to use the special function Φ in the method of Zhang and Chen (13) for arbitrary EOS

$$\Phi(\tilde{\rho}, \tilde{T}) = \sqrt{-\tilde{U}(\tilde{\rho}, \tilde{T})}. \tag{15}$$

In this case, we can rewrite Eq. (13) in the form

$$\mathbf{F} = 2\Phi\nabla\Phi. \tag{16}$$

Zhang and Chen [3] proposed a direct numerical approximation of Eq. (13)

$$\mathbf{F} = \frac{1}{2\alpha h}\sum_{k=1}^{N}\frac{G_k}{G_1}\tilde{U}(\mathbf{x} + \mathbf{e}_k)\mathbf{e}_k, \tag{17}$$

which can be rewritten for symmetric lattices with even values of N as

$$\mathbf{F} = \frac{1}{\alpha}\sum_{k=1}^{N}\frac{G_k}{G_1}\left[\frac{\Phi(\mathbf{x} + \mathbf{e}_k) + \Phi(\mathbf{x} - \mathbf{e}_k)}{2}\right]\left[\frac{\Phi(\mathbf{x} + \mathbf{e}_k) - \Phi(\mathbf{x} - \mathbf{e}_k)}{2h}\right]\mathbf{e}_k. \tag{18}$$

Here, coefficients G_k are the same as in Eq. (11).

On the other hand, the direct numerical approximation of Eq. (16) is also possible [12,30]

$$\mathbf{F} = \frac{1}{\alpha h}\Phi(\mathbf{x})\sum_{k=1}^{N}\frac{G_k}{G_1}\Phi(\mathbf{x} + \mathbf{e}_k)\mathbf{e}_k. \tag{19}$$

This formula can be rewritten for symmetric lattices with even values of N as

$$\mathbf{F} = \frac{1}{\alpha}\Phi(\mathbf{x})\sum_{k=1}^{N}\frac{G_k}{G_1}\left[\frac{\Phi(\mathbf{x} + \mathbf{e}_k) - \Phi(\mathbf{x} - \mathbf{e}_k)}{2h}\right]\mathbf{e}_k. \tag{20}$$

This approximation of force is different from (18). Namely, the local value of function $\Phi(\mathbf{x})$ at a given node is used in (20) instead of the average values $[\Phi(\mathbf{x} + \mathbf{e}_k) + \Phi(\mathbf{x} - \mathbf{e}_k)]/2$ in (18). Thus, formulas (19) and (20) can be called the local approximation, and formulas (17) and (18) can be called the mean-value approximation.
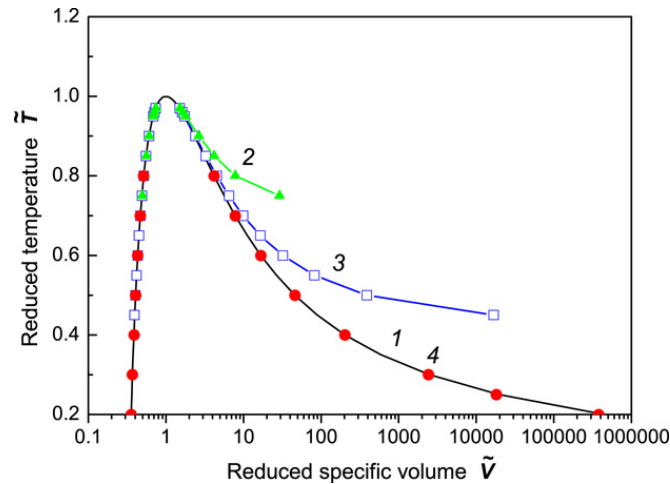
Fig. 3. Coexistence curve for the vdW EOS. Curve *1*—theory (Maxwell rule), curve *2*—mean-value approximation (17), curve *3*—local approximation (19), points *4*—combined approximation (21).

A more general approximation is also possible. It combines formulas (17) and (19) with different weights

$$\mathbf{F} = \frac{1}{\alpha h} \left[A \sum_{k=1}^{N} \frac{G_k}{G_1} \Phi^2(\mathbf{x} + \mathbf{e}_k)\mathbf{e}_k + (1 - 2A)\Phi(\mathbf{x}) \sum_{k=1}^{N} \frac{G_k}{G_1} \Phi(\mathbf{x} + \mathbf{e}_k)\mathbf{e}_k \right]. \tag{21}$$

For $A = 0$, it coincides with the local approximation (19), for $A = 0.5$, with the mean-value approximation (17).

4. Results

4.1. Coexistence curve and surface tension

Fig. 3 shows the coexistence curve for a fluid with the vdW EOS calculated using different approximations of the force (13). The theoretical results are also shown. One can see that the liquid branch of the coexistence curve is reproduced quite well for all approximations. On the other hand, the mean-value approximation (17) faces great problems at the vapor branch. This approximation gives large deviations and calculations become unstable at rather high temperature $\tilde{T} \approx 0.72$. The local approximation (19) is better, but the deviations become progressively larger as the temperature decreases, and the calculations become unstable below the temperature $\tilde{T} \approx 0.45$. Our general approximation (21) can be tuned by the coefficient A. For $A = -0.152$, the simulation results virtually coincide with the theory (for $\tilde{T} \geq 0.4$, the deviations are lower than 0.4%). The stability is also greatly improved. For a flat interface in the stationary case, we can obtain the maximum density ratio larger than 10^7 for the vdW and mKM EOS, and even larger than 10^9 for the C–S EOS. The necessary value of A depends only on the EOS used.

We calculated the surface tension coefficient γ for the vdW EOS at different temperatures. Two methods were used. First, we calculated the pressure difference inside and outside a drop of radius R. A linear dependence on the inverse radius (Laplace law) was obtained

$$P_{\text{in}} - P_{\text{out}} = \frac{\gamma}{R}$$

from which γ can be easily calculated. In the second method, the surface tension was calculated from the expression

$$\gamma = \int_{-\infty}^{\infty} (P_{zz} - P_{xx}) \, \mathrm{d}z,$$

where P_{zz} and P_{xx} are the components of the stress tensor normal and parallel to the flat liquid–vapor interface. Results are shown in Table 1. Here, γ_L and γ_s are the surface tension coefficients calculated using the Laplace law and the integration of the stress difference, respectively. Both methods give very close results. The calculated temperature dependence of the surface tension is $\gamma \sim \left(1 - \tilde{T}\right)^{1.48}$ which is in good agreement with the theoretical result for the vdW EOS $\gamma \sim \left(1 - \tilde{T}\right)^{1.5}$.

4.2. Spurious currents

We investigated the spurious currents arising in simulation of a stationary two-phase state using different EOS. The size of the computational area was 80×80 lattice nodes. A drop with equilibrium radius of 15 lattice nodes was placed in the center. Simulation proceeded until the equilibrium was reached, and the maximum value of the fluid velocity near the vapor–liquid interface was measured. Results are shown in Fig. 4 for the vdW EOS, the mKM EOS and the C–S EOS. For each

Table 1
Surface tension.

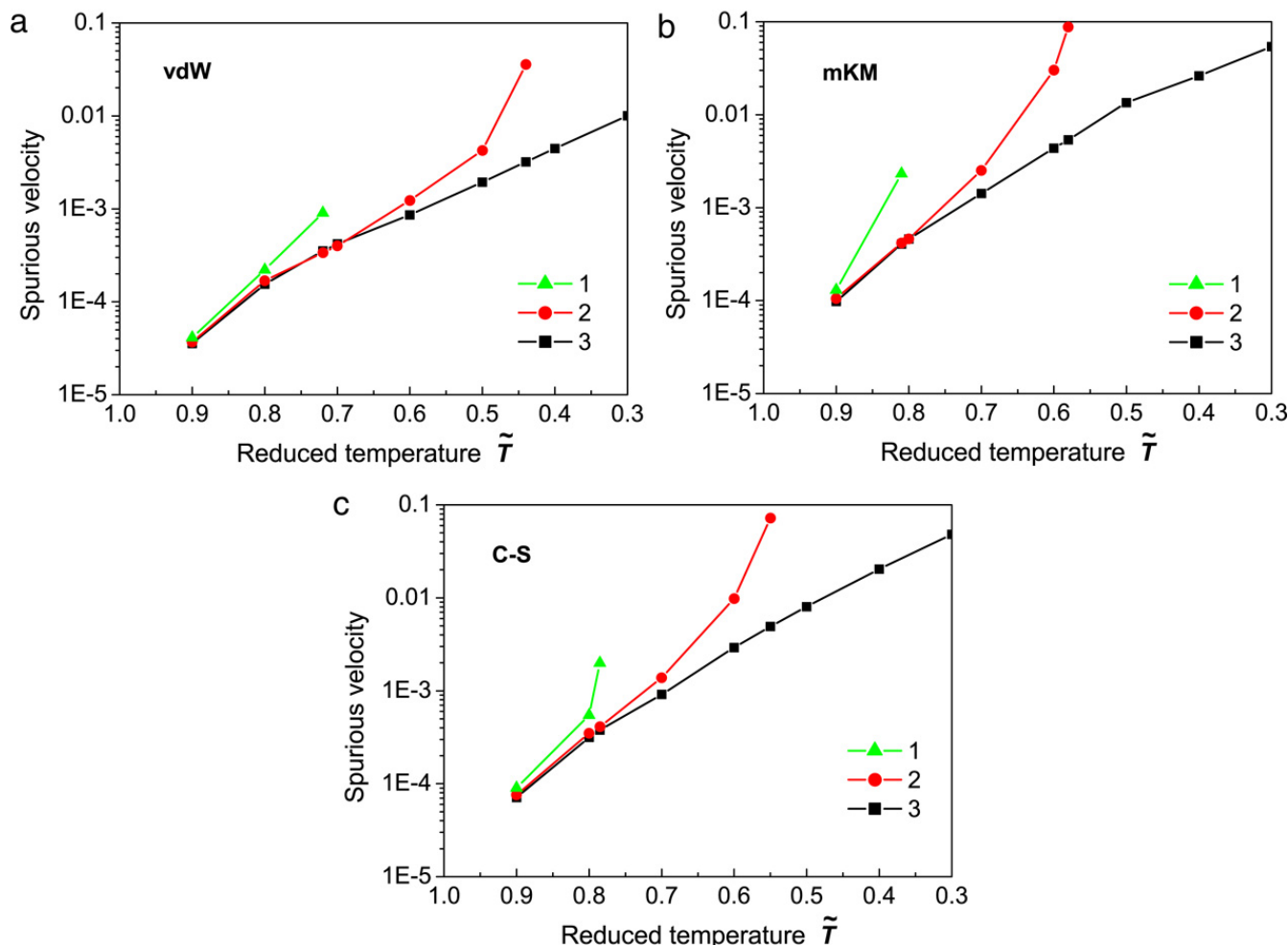| $\tilde{T}$	0.8	0.7	0.6	0.5	0.4
γ_L	0.01494	0.02757	0.04301	0.05983	0.07968
γ_s	0.01555	0.02845	0.04355	0.06035	0.07845

Fig. 4. Spurious velocities at vapor–liquid interface for the vdW EOS (a), mKM EOS (b), and C–S EOS (c). Mean-value approximation (curves 1), local approximation (curves 2), general approximation (curves 3).

EOS, three approximations of the potential gradient (17), (19) and (21) were tested. In all simulations, the body force was included into the LBE using the exact difference method (10).

With the mean-value approximation (17), the lowest temperature that can be achieved is $\tilde{T} = 0.72$ for the vdW EOS, $\tilde{T} = 0.81$ for the mKM EOS, and $\tilde{T} = 0.785$ for the C–S EOS. For lower temperatures, simulations become unstable although the spurious velocities are not extremely high. With the local approximation (19), one can achieve lower temperatures. However, the coexistence curves obtained are incorrect (see Fig. 3 for the vdW EOS). The general approximation (21) again gives the lowest spurious velocities and the best stability of calculations, as can be seen in Fig. 4. Hence, this method is preferable for use in LBE simulations.

4.3. Applications

To illustrate the power of the scheme proposed, we consider three examples. The first one is the last stages of bubble cavitation in a layer of a liquid in a rarefaction wave. The results of simulations of the bubble cavitation in a liquid as an essentially stochastic process are shown in Fig. 5. The size of computational area was 2000×200 lattice nodes. Many microbubbles (Fig. 5b) were initially placed randomly in the liquid layer $-x_0 < x < x_0$. Areas from the left of layer at $x < -x_0$ and from the right of layer at $x > x_0$ were filled with the saturated vapor. The boundaries of calculation area were far enough from the liquid layer. Periodic boundary conditions were used in the y direction. The initial linear distribution of velocity $u_x = u_0 x / x_0$ (Fig. 5a) and the condition $u_y = 0$ were set in two-phase layer at $t = 0$. Then, the evolution of
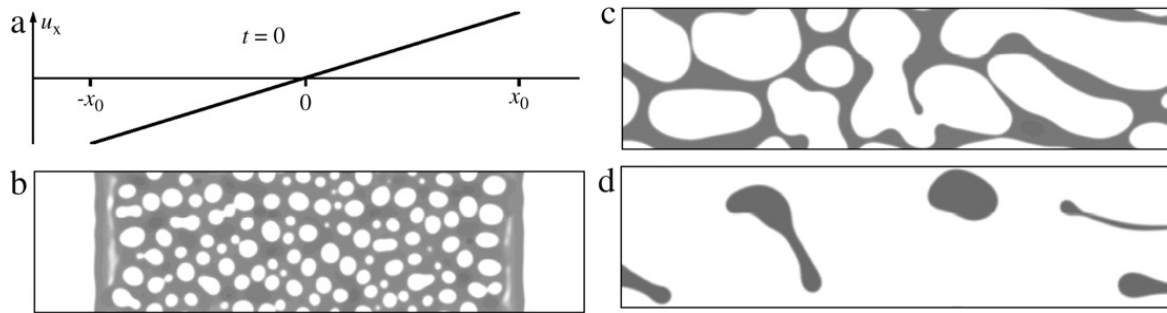
Fig. 5. Last stages of bubble cavitation in a layer of liquid under the conditions of "rarefaction wave". Only central part 1300×200 of the computational area is shown. $x_0 = 500$, $u_0 = 0.15$, $k = 0.01$, $\tau = 0.9$.
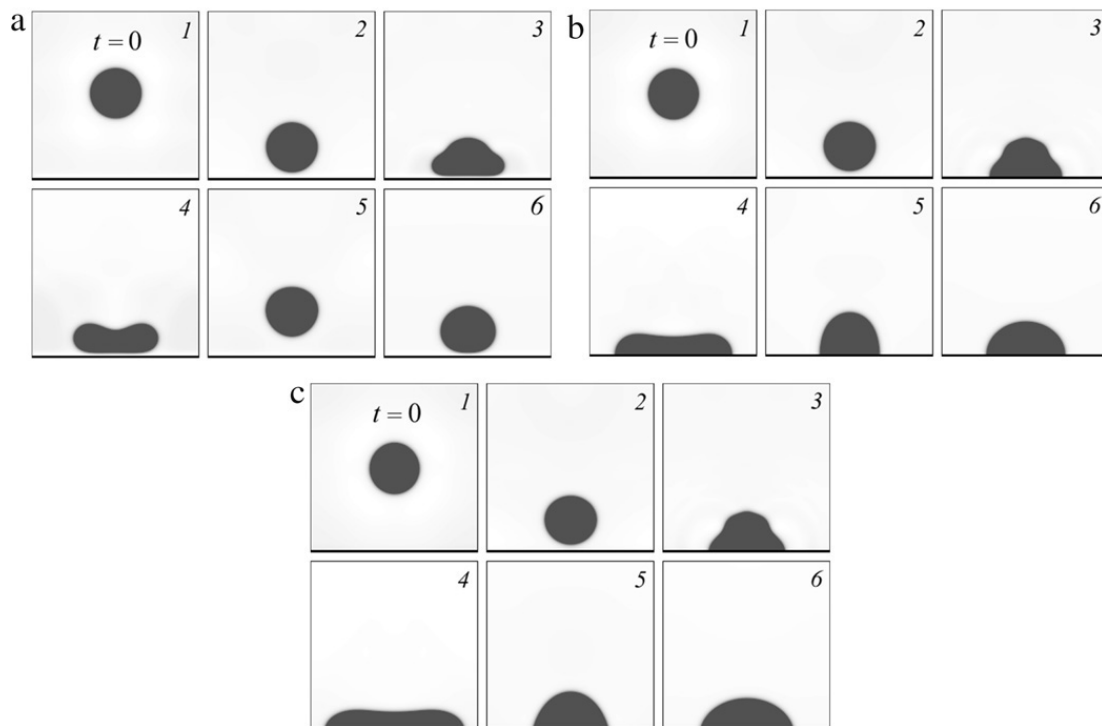

Fig. 6. Free fall of a liquid drop and its collision with a flat rigid surface in gravitational field. (a) Nonwettable surface. (b) Wetting angle $\pi/2$. (c) Wetting angle $< \pi/2$. $\tilde{T} = 0.6$, $k = 0.01$, $\tau = 0.6$.

two-phase flow without external forces was simulated in the isothermal case at $\tilde{T} = 0.8$. The two-phase region expanded, and the fluid flow with bubbles was transformed to a foam structure (Fig. 5c) and at later stages to gas-drop flow (Fig. 5d).

The second example is the simulation of the free fall of a liquid drop and its collision with a flat rigid surface in gravitational field. The results are shown in Fig. 6. For each variant (a), (b) and (c), the final shapes of drops after a long time are shown at last frames (No. 6). The size of computational area was 200×200 lattice nodes. Periodic boundary conditions were used in the x direction. The initial drop radius was 30 lattice nodes. The gravity acceleration was $g = 10^{-5}$ lattice units. In the case of nonwettable wall, the drop initially flattened after collision and then oscillations of form began because of surface tension. If capillary forces are greater than gravitational ones, the drop can jump over the surface (Fig. 6a-5). After a long time, the oscillations stopped because of energy dissipation due to viscosity. The detachment of the drop from the wettable surface (Fig. 6b,c) did not occur. In this case, the oscillations of drop around the stationary shape were observed. The stationary shape was achieved practically after several oscillations.

The third example is the Marangoni effect. This is the onset of a thermocapillary flow because of the temperature dependence of the surface tension coefficient. A liquid film of constant thickness was initially placed between two parallel walls (Fig. 7a). The wetting angle was set to $\pi/2$ (neutral wetting). Then a non-uniform temperature distribution along the film was set, $\tilde{T} = \tilde{T}_0 + \Delta\tilde{T}\sin(\pi x/L)$. Here, L is the length of the film. Across the film, the temperature was assumed constant. The size of computational area was 150×150 lattice nodes. Periodic boundary conditions were used in the y direction. The evolution of the system is shown in Fig. 7. Since the surface tension decreases with an increase of the temperature, liquid was pulled out from the middle (hot) region of the film to the colder ends. The film got thinner in the middle and could break (Fig. 7c) producing two drops which after some oscillations acquired quasiequilibrium shape (Fig. 7,m). Since drops
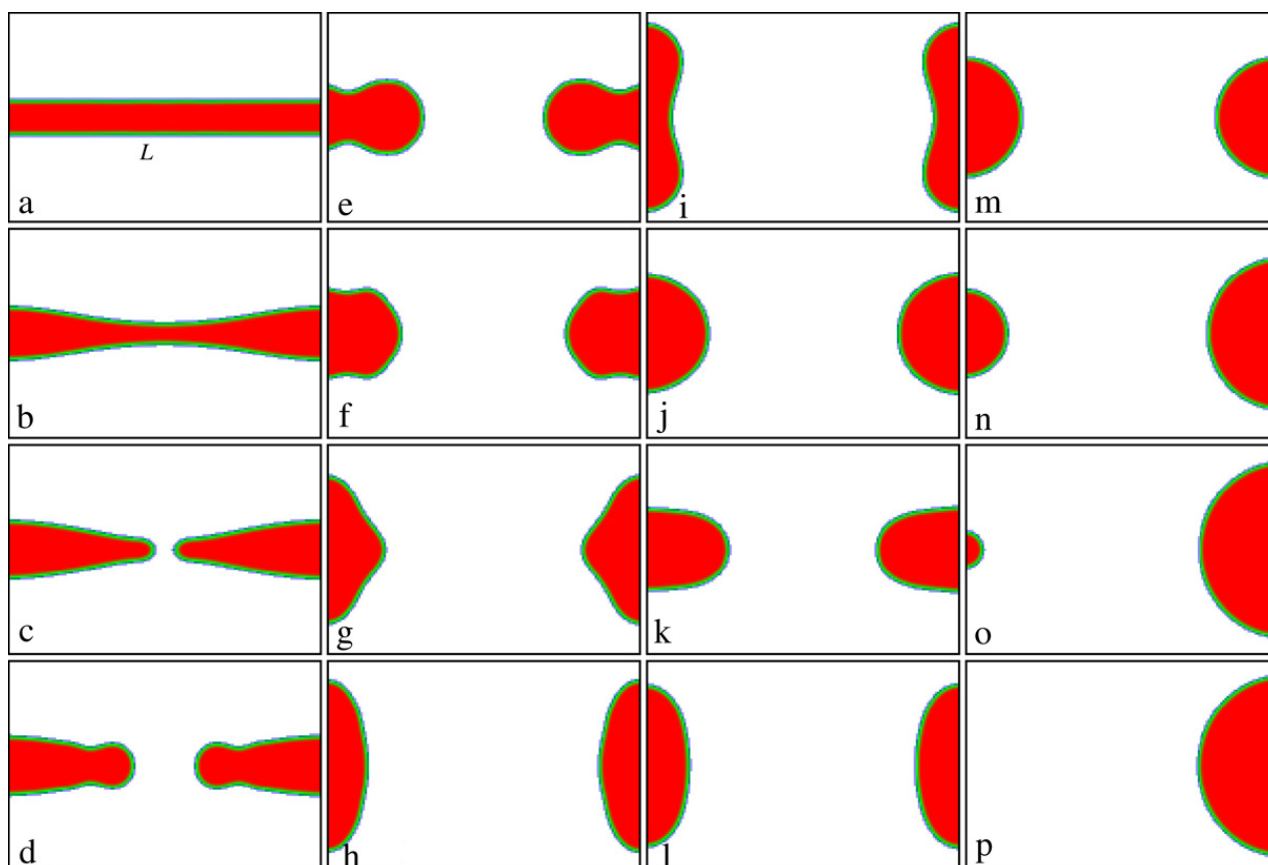
Fig. 7. Marangoni effect. Time $t = 0$ (a), 2500 (b), 3350 (c), 3500 (d), 3800 (e), 4100 (f), 4400 (g), 4600 (h), 5000 (i), 6000 (j), 6500 (k), 8000 (l), 18000 (m), 50000 (n), 58000 (o), 58800 (p) time step units. $\tilde{T}_0 = 0.6$, $\Delta\tilde{T} = 0.018$, $k = 0.00915$, $\tau = 0.55$. Size of frames 150×100 nodes.

were not exactly the same, another interesting phenomenon was then observed. The pressure of vapor was lower than the corresponding saturated value for the smaller drop, therefore, this drop evaporated. On the other hand, the pressure of vapor was higher than the saturated value for the larger drop, and the larger drop grew. This process accelerated as the size difference became larger, and finally only one hemispherical drop remained (Fig. 7p).

5. Conclusions

In summary, we proposed a method of correct incorporation of arbitrary EOS into LBE model. This was achieved using two ideas. First, a new general approximation of the gradient of special potential was introduced. Second, a new method to take into account the action of body forces was developed—the exact difference method.

Our scheme allows one to obtain the density ratio in a stationary case as high as 10^7 for the van der Waals and the mKM EOS, and 10^9 for the Carnahan–Starling one. The largest deviations of the specific volume at the coexistence curve from theoretical values for van der Waals EOS are lower than 0.4% (for $T \geq 0.4T_c$). Spurious velocities are also substantially reduced.

A possible limitation of the method proposed is that the sound speed $\tilde{c}_s = \sqrt{k\,\partial\tilde{P}/\partial\tilde{\rho}}$ in the vapor phase may become small. Hence, only flows with sufficiently small velocity $u < \tilde{c}_s h/\Delta t$ can be simulated reliably.

This new variant of incorporation of arbitrary EOS in the LBE method is very simple and can be used to simulate a wide variety of flows where phase interfaces are present or possibility of phase transitions is important. We used this method to simulate the process of last stages of bubble cavitation when the volume concentration of vapor phase became large, collisions of liquid drops with a rigid surface in gravitational field, and the Marangoni effect.

References

[1] X. Shan, H. Chen, Lattice Boltzmann model for simulating flows with multiple phases and components, Physical Review E 47 (3) (1993) 1815–1819.
[2] M.R. Swift, W.R. Osborn, J.M. Yeomans, Lattice Boltzmann simulation of nonideal fluids, Physical Review Letters 75 (5) (1995) 830–833.
[3] R. Zhang, H. Chen, Lattice Boltzmann method for simulations of liquid–vapor thermal flows, Physical Review E 67 (6) (2003) 066711.
[4] T. Inamuro, T. Ogata, S. Tajima, N. Konishi, A lattice Boltzmann method for incompressible two-phase flows with large density differences, Journal of Computational Physics 198 (2004) 628–644.
[5] H. Zheng, C. Shu, Y. Chew, A lattice Boltzmann model for multiphase flows with large density ratio, Journal of Computational Physics 218 (1) (2006) 353–371.

[6] T. Lee, P. Fischer, Eliminating parasitic currents in the lattice Boltzmann method for nonideal gases, Physical Review E 74 (4) (2006) 046709.
[7] X. Shan, Analysis and reduction of the spurious current in a class of multiphase lattice Boltzmann models, Physical Review E 73 (4) (2006) 047701.
[8] M. Sbragaglia, R. Benzi, L. Biferale, S. Succi, K. Sugiyama, F. Toschi, Generalized lattice Boltzmann method with multirange pseudopotential, Physical Review E 75 (2) (2007) 026702.
[9] J. Zhang, B. Li, D.Y. Kwok, Mean-field free-energy approach to the lattice Boltzmann method for liquid–vapor and solid-fluid interfaces thermal flows, Physical Review E 69 (3) (2004) 032602.
[10] P. Yuan, L. Schaefer, Equations of state in a lattice Boltzmann model, Physics of Fluids 18 (4) (2006) 042101.
[11] A.L. Kupershtokh, New method of incorporating a body force term into the lattice Boltzmann equation, in: Proc. 5th International EHD Workshop, University of Poitiers, Poitiers, France, 2004, pp. 241–246.
[12] A.L. Kupershtokh, Simulation of flows with liquid–vapor interfaces by the lattice Boltzmann method, Vestnik NGU (Quarterly Journal of Novosibirsk State Univ.), Series: Math., Mech. and Informatics 5 (3) (2005) 29–42. (in Russian).
[13] A.L. Kupershtokh, Calculations of the action of electric forces in the lattice Boltzmann equation method using the difference of equilibrium distribution functions, in: Proc. 7th Int. Conf. on Modern Problems of Electrophysics and Electrohydrodynamics of Liquids, St. Petersburg State University, St. Petersburg, Russia, 2003, pp. 152–155.
[14] A.L. Kupershtokh, Incorporating a body force term into the lattice Boltzmann equation, Vestnik NGU (Quarterly Journal of Novosibirsk State Univ.), Series: Math., Mech. and Informatics 4 (2) (2004) 75–96. (in Russian).
[15] N. Carnahan, K. Starling, Equation of state for nonattracting rigid spheres, Journal of Chemical Physics 51 (2) (1969) 635–636.
[16] A.B. Kaplun, A.B. Meshalkin, Thermodynamic validation of the form of unified equation of state for liquid and gas, High Temperature 41 (3) (2003) 319–326.
[17] A.B. Kaplun, A.B. Meshalkin, Behavior of the heat capacity c_v at the liquid–vapor critical point and in the two-phase region of a thermodynamic system, Doklady Physics 50 (9) (2005) 434–437.
[18] V.P. Skripov, M.Z. Faizullin, Crystal-Liquid-Gas Phase Transitions and Thermodynamic Similarity, Willey-VCH, 2006.
[19] P. Bhatnagar, E.P. Gross, M.K. Krook, A model for collision processes in gases. I. Small amplitude processes in charged and neutral one-component systems, Physical Review 94 (3) (1954) 511–525.
[20] X. He, X. Shan, G.D. Doolen, Discrete Boltzmann equation model for nonideal gases, Physical Review E 57 (1) (1998) R13–R16.
[21] L.-S. Luo, Unified theory of lattice Boltzmann models for nonideal gases, Physical Review Letters 81 (8) (1998) 1618–1621.
[22] L.-S. Luo, Theory of the lattice Boltzmann method: Lattice Boltzmann models for nonideal gases, Physical Review E 62 (4) (2000) 4982–4996.
[23] A.J.C. Ladd, R. Verberg, Lattice-Boltzmann simulations of particle-fluid suspensions, Journal of Statistical Physics 104 (5–6) (2001) 1191–1251.
[24] Z. Guo, C. Zheng, B. Shi, Discrete lattice effects on the forcing term in the lattice Boltzmann method, Physical Review E 65 (4) (2002) 046308.
[25] I. Ginzburg, P.M. Adler, Boundary flow condition analysis for the three-dimensional lattice Boltzmann model, Journal de Physique II France 4 (2) (1994) 191–214.
[26] X. Shan, H. Chen, Simulation of nonideal gases and liquid-gas transitions by the lattice Boltzmann equation, Physical Review E 49 (4) (1994) 2941–2948.
[27] X. He, G.D. Doolen, Thermodynamic foundations of kinetic theory and lattice Boltzmann models for multiphase flows, Journal of Statistical Physics 107 (1–2) (2002) 309–328.
[28] R.R. Nourgaliev, T.N. Dinh, T.G. Theofanous, D. Joseph, The lattice Boltzmann equation method: Theoretical interpretation, numerics and implications, International Journal of Multiphase Flow 29 (1) (2003) 117–169.
[29] A.L. Kupershtokh, C. Stamatelatos, D.P. Agoris, Stochastic model of partial discharge activity in liquid and solid dielectrics, in: Proc. IEEE 15th International Conf. on Dielectric Liquids, University of Coimbra, Coimbra, Portugal, 2005, pp. 135–138.
[30] A.L. Kupershtokh, D.I. Karpov, D.A. Medvedev, C. Stamatelatos, V.P. Charalambakos, E.C. Pyrgioti, D.P. Agoris, Stochastic models of partial discharge activity in solid and liquid dielectrics, IET Science, Measurement & Technology 1 (6) (2007) 303–311.